

# Fate of the classical false vacuum

Sz. Borsányi<sup>a,1</sup>, A. Patkós<sup>a,b,2</sup>, J. Polonyi<sup>a,b,3</sup>, Zs. Szép<sup>a,4</sup>

<sup>a</sup>*Department of Atomic Physics*

*Eötvös University, Budapest, Hungary*

<sup>b</sup>*Lab. de Physique Théorique*

*Univ. L. Pasteur, Strasbourg, France*

(April 10, 2000)

Thermalisation of configurations with initial white noise power spectrum is studied in numerical simulations of a one-component  $\Phi^4$  theory in 2+1 dimensions, coupled to a small amplitude homogenous external field. The study is performed for energy densities corresponding to the broken symmetry phase of the system in equilibrium. The effective equation of the order parameter motion is reconstructed from its trajectory which starts from an initial value near the metastable point and ends in the stable ground state. This phenomenological theory quantitatively accounts for the decay of the false vacuum. The large amplitude transition of the order parameter between the two minima displays characteristics reflecting the dynamical effect of the Maxwell construction.

## I. INTRODUCTION

The reach of equilibrium from a metastable state covers a large number of interesting effects from instabilities observed in the mixed phase of first order phase transitions [1] to the inflation in the early Universe [2]. The final state is reached in an irreversible process, the description of this relaxation relies on out-of-equilibrium dynamics of field theories.

The decay of metastable states is usually discussed in the framework of the nucleation scenario [3]. It has been implemented in the form of saddle point expansions in classical [4], and quantum systems [5]. This large amplitude instability is, however, only the first of the possible instabilities, suggested by mean field analysis, and consists of the creation of a bubble of the true vacuum larger than the critical size, embedded into the false one.

Another possibility, the instability against fluctuations with infinitesimal amplitude leads to the spinodal phase separation. A recent observation made it clear that soft fluctuations of these inhomogeneous unstable modes generate in equilibrium the Maxwell construction by their tree-level contribution to the renormalization group flow [6]. The fluctuation induced flatness of the effective potential suggests the dominance of spinodal phase separation in equilibrium.

Since the type of instability one observes, might depend essentially on the time scale of the observation, a detailed investigation of the time evolution can separate the effects of the two kinds of instabilities. This is made possible by large scale computer simulations of the thermalisation process in closed systems.

Another question, left open by the Maxwell construction in equilibrium, concerns the structure of the vacuum with spontaneous symmetry breaking. In fact, the effective potential is related to the probability distribution of the order parameter and the Maxwell-cut applied to the former suggests that the latter is also degenerate in the mixed phase. Either we accept that the vacua with spontaneously broken symmetry correspond overwhelmingly to the mixed phase or a dynamical mechanism is sought to eliminate the mixed phase from among the final states of the time evolution.

In cosmology different slow-roll scenarios of inflation are being considered. Recent studies of the dynamics of inflaton fields with large number of components (large  $N$  limit) display a dynamical version of the Maxwell construction [7]. The Hartree type solution of the quantum dynamical equations leads to the conclusion that the order parameter might get rest with finite probability at any value smaller than the position of the stable minimum of the tree level effective potential, corresponding to the stabilisation of a mixed state.

Detailed investigations of the thermalisation phenomenon were performed also in noisy-damped systems, coupled to an external heat bath [8–11]. The relaxation to thermal equilibrium of the space averaged scalar field (the order parameter) starting from metastable initial values has been thoroughly investigated. In these simulations the damping coefficient is treated as an external control parameter. Using the numerical solution of the corresponding Langevin-equations the validity range of the analytical results for the homogenous nucleation mechanism has been explored.

---

<sup>1</sup>[mazsx@cleopatra.elte.hu](mailto:mazsx@cleopatra.elte.hu)

<sup>2</sup>[patkos@ludens.elte.hu](mailto:patkos@ludens.elte.hu)

<sup>3</sup>[polonyi@fresnel.u-strasbg.fr](mailto:polonyi@fresnel.u-strasbg.fr)

<sup>4</sup>[szepzs@cleopatra.elte.hu](mailto:szepzs@cleopatra.elte.hu)

In this paper we focus on an alternative description of the decay process of the metastable vacuum state. The process is described exclusively in terms of the homogenous order parameter (OP) mode. The evolution of the OP is studied in interaction with the rest of the system as described by the reversible dynamical equations of motion of the full system. Careful analysis of its dynamics allows us to explore the effects of both kinds of instabilities. The transition of the order parameter from the metastable to the stable vacuum is induced by a homogenous external “magnetic” field, whose strength is systematically reduced. No random noise is introduced to represent any external heat bath, the friction coefficient of the effective order parameter dynamics is determined internally.

Our results offer a “dualistic” resolution of the competition between the nucleation and the spinodal phase separation mechanisms in establishing the true equilibrium. On the one hand, we find that the statistical features of the decay of the false vacuum agree with the results obtained by expanding around the critical bubble. The microscopic mapping of the field configurations during the relaxation supports the bubble creation scenario. On the other hand, the effective OP-theory displays the presence of soft modes and produces dynamically a Maxwell-cut when the time dependence of the transition trajectory is described in the effective theory. We find that the larger is the system the smaller is the external field which is able to produce the instability. For infinite systems an infinitesimal field pushes the system through the Maxwell-cut, where no force is experienced by the OP. Therefore it will not stop before reaching the true homogenous ground state passing by the mixed states with constant velocity.

Our model, a spacelike lattice regulated scalar  $\Phi^4$  field theory in its broken symmetry phase is introduced in Section 2. In Section 3 we describe the evolution of the system starting from order parameter values near a metastable point which relaxes first to this state under the combined effect of parametric resonances and spinodal instabilities. The second stage of the transition to the stable ground state is the actual focus of our paper.

Characteristic intervals of the observed order parameter trajectory are reinterpreted as being the solutions of some effective point-particle equation of motion, which displays dissipation effects explicitly. Our approach can be understood also as the real-time version of the lowest mode approximation used for the estimation of finite size dependences in Euclidean field theory [12,13]. In this sense our approach can be considered also as the numerical implementation of a real time renormalisation group strategy.

One of our principal goals is to reconstruct the thermodynamics of the “OP-ensemble” on the (meta)stable branches of the OP-trajectory (Section 4). Its dissipative dynamical equations near equilibria will be established. On the transition trajectory we shall elaborate on the presence of the Maxwell construction in the effective dynamics describing the motion after nucleation (Section 5). The statistical aspects of the approach to the equilibrium are established for reference and comparison in an Appendix. The conclusions of this investigation are summarised in Section 6.

The results of this study can be usefully compared with classical investigations of metastability and nucleation in the kinetic Ising model [14]. This system has first order dissipative dynamics by its definition. Still several relaxation features of the kinetic Ising model are comparable to our findings, since the “numerical experiment” performed in the two models are essentially the same. Especially, the relaxation function of [14] is simply related to the order parameter we focus our attention. In both cases in the mechanism of the bubble growth the aggregation of spontaneously generated small size regions of the true ground state to its surface plays important role.

## II. CLASSICAL CUT-OFF $\Phi^4$ -THEORY ON LATTICE

The energy functional of a classical system in a two-dimensional box of size  $L_d$  coupled to an external magnetic field of strength  $h_d$  is of the following form:

$$E_d = \int d^2x_d \left[ \frac{1}{2} \left( \frac{d\Phi_d}{dt_d} \right)^2 + \frac{1}{2} (\nabla_d \Phi_d)^2 + \frac{1}{2} m^2 \Phi_d^2 + \frac{1}{24} \lambda \Phi_d^4 - h_d \Phi_d \right]. \quad (2.1)$$

The index  $d$  is introduced to distinguish the dimensionfull quantities from the dimensionless ones, defined by the relations (for  $m^2 < 0$ ):

$$\begin{aligned} t &= t_d |m|, & x &= x_d |m|, \\ \Phi &= \sqrt{\frac{\lambda}{6}} \frac{1}{|m|} \Phi_d, & h &= \sqrt{\frac{\lambda}{6}} \frac{1}{|m|^3} h_d. \end{aligned} \quad (2.2)$$

For the spatial discretisation one introduces a lattice of size

$$L_d = N a_d = N a \frac{1}{|m|}. \quad (2.3)$$

The energy functional of the lattice system can be written as

$$\begin{aligned} E \equiv \frac{\lambda}{6|m|^2} E_d = \frac{a_t^2}{a_t^2} \sum_{\mathbf{n}} & \left[ \frac{1}{2} (\Phi_{\mathbf{n}}(t) - \Phi_{\mathbf{n}}(t - a_t))^2 + \frac{a_t^2}{2a^2} \sum_{\mathbf{i}} (\Phi_{\mathbf{n}+\mathbf{i}} - \Phi_{\mathbf{n}})^2 \right. \\ & \left. - \frac{a_t^2}{2} \Phi_{\mathbf{n}}^2 + \frac{a_t^2}{4} \Phi_{\mathbf{n}}^4 - a_t^2 h \Phi_{\mathbf{n}} \right]. \end{aligned} \quad (2.4)$$

(Here we have introduced the dimensionless time-step  $a_t$ , which should be chosen much smaller than  $a$ , and  $\mathbf{n}$  denotes the lattice site vectors.) The equation of motion to be solved numerically is the following:

$$\begin{aligned}\Phi_{\mathbf{n}}(t + a_t) + \Phi_{\mathbf{n}}(t - a_t) - 2\Phi_{\mathbf{n}}(t) - \frac{a_t^2}{a^2} \sum_i (\Phi_{\mathbf{n}+\hat{\mathbf{i}}}(t) + \Phi_{\mathbf{n}-\hat{\mathbf{i}}}(t) - 2\Phi_{\mathbf{n}}(t)) \\ + a_t^2(-\Phi_{\mathbf{n}} + \Phi_{\mathbf{n}}^3 - h) = 0.\end{aligned}\quad (2.5)$$

The initial conditions for Eq.(2.5) were chosen as

$$\dot{\Phi}_{\mathbf{n}}(t = 0) = 0, \quad \Phi_{\mathbf{n}}(t = 0) = \Phi_0 + \xi\Phi_1. \quad (2.6)$$

The random variable  $\xi$  is distributed evenly on the interval  $(-1, 1)$ . Therefore the starting OP-value is  $\Phi_0$ . The energy density  $E/Na^2$  is controlled through the magnitude of  $\Phi_1$ . In this study we have chosen  $\Phi_0 = 0.815$  and  $\Phi_1 = 4/\sqrt{6}$ . The latter corresponds to a temperature value  $T_i = 0.57$  in the metastable equilibrium (from Eq.(4.5)). This value is much below the critical temperature of the system ( $T_c \simeq 1.5T_i$ ). It has been checked that at this energy density all other choices of  $\Phi_0 > 0$ , for fixed  $h$ , find a unique metastable equilibrium.

Eq.(2.5) was solved with  $a = 1$  and with typical  $a_t$  values in the range (0.01-0.09). It has been checked that the statistical characteristics of the time evolution is not sensitive to the variation of  $a_t$ , though the “release” time (the moment of the transition from metastability to the true ground state) in any single run with given initial conditions might change considerably under the variation of  $a_t/a$ . Three lattice sizes were systematically explored:  $N = 64, 128, 256$ . Several single runs were performed also for  $N = 512$  and  $N = 1000$  with the aim to analyze in more detail some self-averaging physical quantities on different portions of the trajectory under the assumption of the ergodicity of the system. The magnetic field  $h$  inducing the transition was varied in the range  $h \in -(0, 0.08)/\sqrt{6}$ . For the reconstruction of the effective potential felt by the OP also positive values were chosen up to  $h = 0.5/\sqrt{6}$ . The smaller the value of  $|h|$  was fixed, the longer the “release” times have grown on the average. For this reason also the runs were prolonged with decreasing  $|h|$ , and for the smallest  $|h|$  the length of a run reached up to  $(10^6 - 10^7)|m|^{-1}$  until the transition took place.

Table I shows the transition event statistics for each  $(h, N)$  pair, used in this analysis. On smaller lattices, for a few  $h$  values very large number of transitions were observed, in order to clarify the nature of the corrections to the nucleation mechanism. For the largest systems at the smallest  $h$  the event rate was 1-2/day/ 400 MHz-processor.

$-\sqrt{6}h$	N		
	64	128	256
0.028	-	-	10
0.03	-	6	46
0.032	-	-	93
0.035	-	71	49
0.037	4	-	38
0.04	268	109	400
0.045	141	27	91
0.05	356	93	83
0.055	182	173	1158
0.06	10529	200	808
0.065	368	200	553
0.07	12	200	-
0.075	-	200	-
0.08	5328	1624	1082
0.1	80	-	-
0.15	100	-	-

TABLE I. Nucleation event statistics for different lattice sizes (N) and external magnetic fields (h).

### III. TIME-HISTORY OF THE ORDER PARAMETER

A typical OP-history is displayed in Fig.1. In the same figure we show also the history of the OP mean square (MS)-fluctuation ( $\langle \Phi^2 \rangle - \langle \Phi \rangle^2$ ) and of its third moment ( $\langle (\Phi - \langle \Phi \rangle)^3 \rangle$ ). The evolution of the non-zero  $\mathbf{k}$  modes is demonstrated in Fig.2, where the averaged kinetic energy content of the  $|\mathbf{k}| < 2.5$  and  $|\mathbf{k}| > 2.5$  regions is followed. Although the separation value is somewhat arbitrary, namely it divides into two nearly equal groups the spatial frequencies available in the lattice system, the figure demonstrates the most important features of the evolution of the power in the low- $|\mathbf{k}|$  and high- $|\mathbf{k}|$  modes.

In general, five qualitatively distinct parts of the trajectory can be distinguished, although some of the first three might be missing for some initial configurations and/or magnetic field strengths.

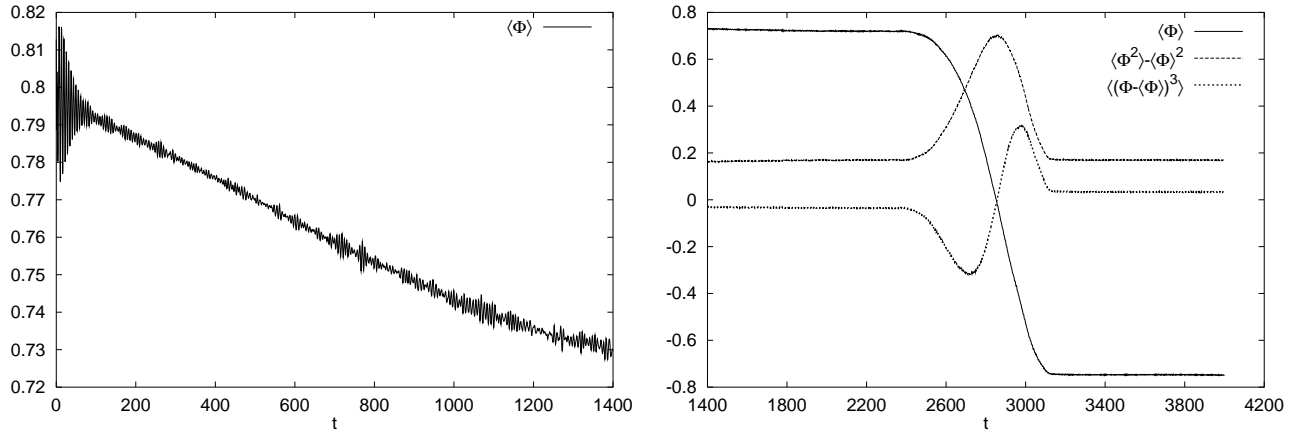


FIG. 1. The time evolution of the order parameter, its MS fluctuation and the third moment. The example is selected from runs on a  $N = 512$  lattice with  $h = -0.04/\sqrt{6}$  external source strength.

The OP-motion usually starts with large amplitude damped oscillations. The “white noise” initial condition of Eq.(2.6) corresponds to a  $\mathbf{k}$ -independent Fourier amplitude distribution, therefore the initial distribution of the kinetic energy is  $\sim \omega^2(|\mathbf{k}|)$ . During this period, in the power spectrum of the kinetic energy, first a single sharp peak shows up at a resonating  $|\mathbf{k}|$ -value ( $|\mathbf{k}| \sim 1.5$ ), which breaks up into several peaks ( $|\mathbf{k}| < 1$ ) at later times due to the non-linear interaction of the modes. At the end of the first period the whole  $|\mathbf{k}| < 1$  range gets increased power, the  $|\mathbf{k}| > 1.5$  part of the power spectrum does not seem to change.

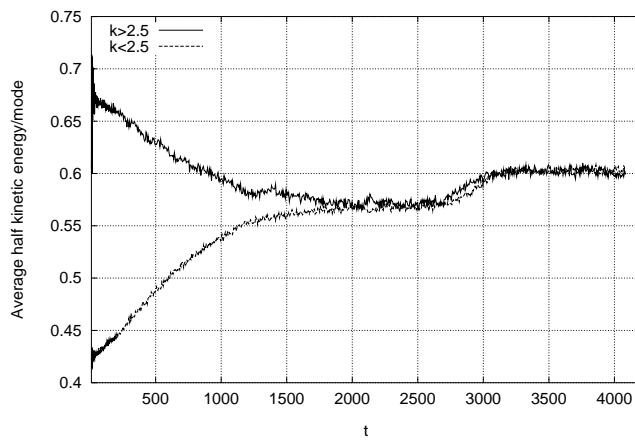


FIG. 2. The time evolution of the kinetic energy content of the  $|\mathbf{k}| > 2.5$  and  $|\mathbf{k}| < 2.5$  regions averaged over the corresponding  $|\mathbf{k}|$ -intervals. The example is the same as in Fig. 1.

Next a slow, almost linear (modulated) decrease of the OP follows. At the same time its MS fluctuation increases linearly. In Fig.2 an energy flow towards the low- $|\mathbf{k}|$  part can be observed, which proceeds through the excitation of single modes in this part. As a result the minimum of the effective potential is continuously shifted to smaller  $\Phi$ -values, as if the temperature would gradually increase (see the left part of Fig.1). The full (microscopic) kinetic energy density shows in this period less than 5% variation. In view of the picture based on the Maxwell construction it is rather surprising that independently of the initial conditions the OP converges towards a well-defined absolute value, depending only on the total energy density.

On the third portion the average value of the OP and its moments stay constant (see the right picture in Fig.1). The average energy content of the low and high- $|\mathbf{k}|$  part of the spectra is nearly the same. This suggests the establishment of a sort of thermal (meta)equilibrium.

In terms of the terminology introduced for the inflation, the first period leading to this (quasi) -stationary state can be called *preheating*, and the second *reheating*. Directly before the moment of the transition to the true vacuum a peak appears in the power spectrum in the narrow neighbourhood of  $\mathbf{k} = 0$  with varying position in time. On the snapshots of the real space configurations a set of randomly distributed small bubbles of the true ground state appear with a radius increasing in time, until one of the bubbles exceeds the critical size.

The fourth portion of the motion is the transition itself. The value of the OP MS-fluctuation increases by about a factor of three and the temporal width of this transient increase measures very well the transition time. The transition time decreases on larger lattices, the height of the jump in the OP-fluctuation is not sensitive to the lattice size. Also the third reduced moment shows a characteristic variation. An increase of the temperature proceeds smoothly during the transition of the OP to its stable value (Fig.2). The slight separation of the two curves in Fig.2 gives a feeling on the degree of uniformity of the temperature variation of the different modes.

The last portion of the trajectory represents stable (thermalised) oscillations around the true ground state. Here a complete equilibration of the power spectrum can be observed (see Fig.2) corresponding to a somewhat increased temperature ( $T \sim 0.6$ ).

#### IV. MOTION NEAR THE (META)STABLE POINT

Our analysis of the motion around the (meta)stable value of the order parameter explores the consequences of assuming the ergodicity hypothesis for a finite time interval. We also wish to detect signatures of the metastability in the period directly preceding the start of the transition of the order parameter to the stable position.

We reconstruct the following phenomenological Newton-type equation of motion for the order parameter based on its trajectory computed from the microscopical equations:

$$\ddot{\Phi}_d + \eta_d(\Phi_d)\dot{\Phi}_d - h_d + \frac{dV_{\text{eff}}(\Phi_d)}{d\Phi_d} = \zeta_d, \quad (4.1)$$

where  $\zeta_d$  is a noise term. In the corresponding dimensionless equation of motion the following new rescaled quantities will appear:

$$\eta_d = |m|\eta, \quad \zeta_d = \zeta|m|^3\sqrt{\frac{6}{\lambda}}. \quad (4.2)$$

The region of the order parameter space visited by the system was divided into small bins and Eq. (4.1) was fitted within each of them without the noise term. Once the functions  $\eta(\Phi)$  and  $f(\Phi) \equiv -h + V'_{\text{eff}}(\Phi)$  are determined, the moments of the noise can be identified with the corresponding moments of the deviation at a given time of the left hand side of the equation of motion (4.1), evaluated with the fitted  $\eta(\Phi)$  and  $f(\Phi)$ , from zero.

The effective equation of motion can be thought to result from the application of a “molecular dynamical renormalization group”, to our microscopical equations. The blocking in space is performed by projecting the field configuration  $\Phi(\mathbf{x}, t)$  on the OP  $\Phi(t)$ . It represents the infrared (IR) end point of such a blocking whose effective theory is now reconstructed from the actual time dependence found numerically.

The *effective force*  $f(\Phi)$  calculated from the time-average of the oscillatory motion around the equilibrium, under the assumption of ergodicity, should agree with the force coming from the theoretically determined finite temperature effective potential calculated perturbatively in the cut-off two-dimensional field theory for some appropriately chosen value of the temperature [15]. With one-loop accuracy the expected equality reads:

$$f(\Phi)_{\text{measured}} = -h + \frac{d}{d\Phi} \left[ V(\Phi) + \frac{T}{8\pi} V''(\Phi) \left( 1 + \log \frac{\Lambda^2}{V''(\Phi)} \right) \right]_{\text{theory}} + \mathcal{O}(T^2). \quad (4.3)$$

The expressions on the right hand side of this equation are connected to the dimensionfull quantities of the original one-loop computation in the following way:

$$T = \frac{\lambda}{6|m|^2} T_d, \quad V(\Phi) = -\frac{1}{2}\Phi^2 + \frac{1}{4}\Phi^4 = \frac{\lambda}{6|m|^2} V_d, \quad \Lambda = \frac{\pi}{a}. \quad (4.4)$$

The dimensionless temperature is defined by the time-average of the kinetic energy based on the assumption that in the effective theory of the OP it has the usual expression in terms of  $\dot{\Phi}(t)$ :

$$\lim_{t \rightarrow \infty} \frac{1}{t} \int_0^t dt' \frac{1}{2} (\dot{\Phi}(t', x))^2 \equiv \frac{1}{2} \overline{\dot{\Phi}^2}^t = \frac{T}{2}. \quad (4.5)$$

One should note that this definition in the dimensionfull version implies a ‘‘Boltzmann-constant’’,  $|m|^2$  multiplying  $T_d$ .

By measuring the order parameter average for different values of the external field  $h$  we obtain the magnetisation curve of the system. In the numerical work we restarted the computation at different values of the external magnetic field but one might as well change  $h$  adiabatically and measure the force law at each (quasi)equilibrium point. The results should agree in the stable regime, up to the phenomenon of the hysteresis. The resulting curve can be viewed as the numerical Legendre transformation by identifying the external source  $h$  with the derivative of the effective potential,

$$-h + V'_{\text{eff}}(\langle \Phi \rangle_{h,\text{measured}}) = 0. \quad (4.6)$$

It was found that  $f(\Phi)_{\text{measured}}$  is always vanishing at  $\Phi = \langle \Phi \rangle_{h,\text{measured}}$ , thus the force acting on the order parameter at the equilibrium position  $\langle \Phi \rangle_h$  induced by the external source  $h$  is indeed always  $-V'_{\text{eff}}(\langle \Phi \rangle_h)$ .

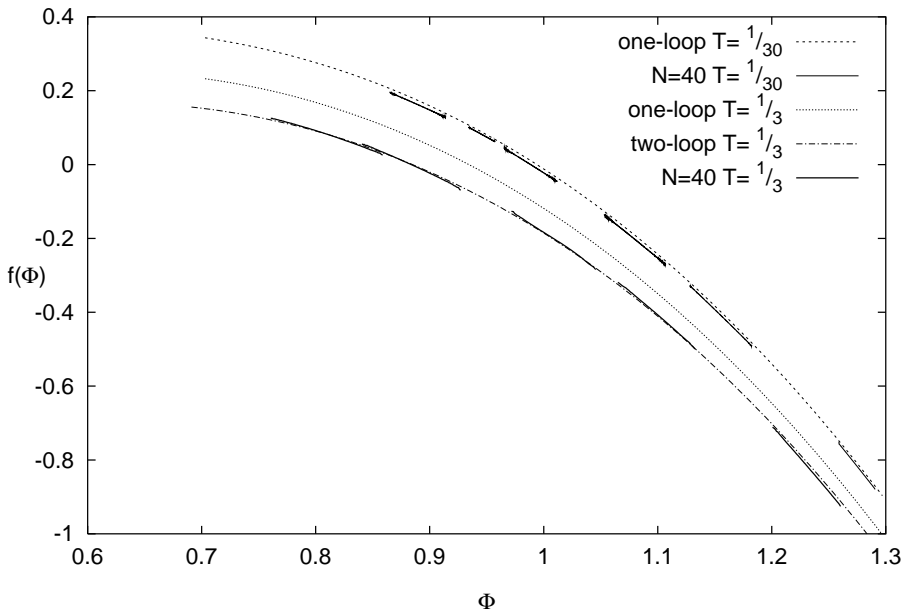


FIG. 3. The force  $f(\Phi)$  as the function of the order parameter on  $40 \times 40$  lattices with  $T = 1/30$  and  $1/3$ . The force is measured by shifting the center of motion to different  $\Phi$  values by applying appropriate  $h$  fields to the system. The finite size effects are negligible, see text. For comparison we display the force arising from the derivative of the one-loop and for  $T = 1/3$  also of the two-loop expressions of the effective potential.

The two sides of the relation (4.3) are shown in Fig.3. To the values of the external field used in preparing Fig.3 ( $h\sqrt{6} = -0.5, -0.02, 0, 0.5, 1, 2$ ) single runs were selected by the requirement that the system stayed in the metastable vacuum up to the time  $10^6$ . The force shown in Fig.3 demonstrates that not only the equilibrium positions but also the fluctuations of the OP are governed by the *static* effective potential. Similar measurements, performed on  $100 \times 100$  lattices showed no finite size effects in the stable regime,  $h > 0$ . The error of  $f(\Phi)$  is not shown in the Figure, since the typical values ( $\sim 0.004$  for  $T = 1/3$  and  $\sim 0.002$  for  $T = 1/30$ ) are too small to be displayed.

Another piece in the effective equation of motion (4.1) is the *friction term* whose presence indicates the dynamical breakdown of the time inversion symmetry. The friction coefficient  $\eta(\Phi)$  proves clearly non-vanishing and shows only weak dependence on the actual value of the OP around its equilibrium position. The breakdown of the time-reflection symmetry in a closed system must arise only in presence of infinitely many degrees of freedom. Till then only statements on the Poincaré-time can be made. Thus our non-zero results for  $\eta$  require further clarifications.

The point is that there are two types of infinities, controlled by the *temporal* UV and the IR cutoffs, respectively. The spontaneous symmetry breaking is driven by the IR modes, and the non-trivial minima of the potential energy arise from the presence of infinitely many degrees of freedom in the IR (thermodynamical limit). On the contrary, the dynamical symmetry breaking [16] is the result of the effects of the derivative terms in the action and the infinitely many UV modes (continuum limit). The breakdown of the time inversion, being related to a time-derivative term in the effective equation of motion, should come from the UV, the short time behaviour of the system.

In fact, one expects no friction when the UV cutoff,  $a_t$  is small enough,

$$a_t < \tau = \frac{2\pi}{\sqrt{\frac{8}{a_s^2} + 2}} + \mathcal{O}(T), \quad (4.7)$$

where  $\tau$  is the time scale of the fastest mode in the system. The right hand side relation of Eq.(4.7) gives the maximal frequency from the dispersion relation  $p_0^2 = 4(\sin^2 p_x a/2 + \sin^2 p_y a/2)/a^2 + M^2(T)$  of the lattice hamiltonian system for fixed  $a$  in the limit  $a_t \rightarrow 0$ . The fast modes absorb energy from the OP in a single time step for  $a_t > \tau$ , and the friction term should appear in the effective equation of motion.

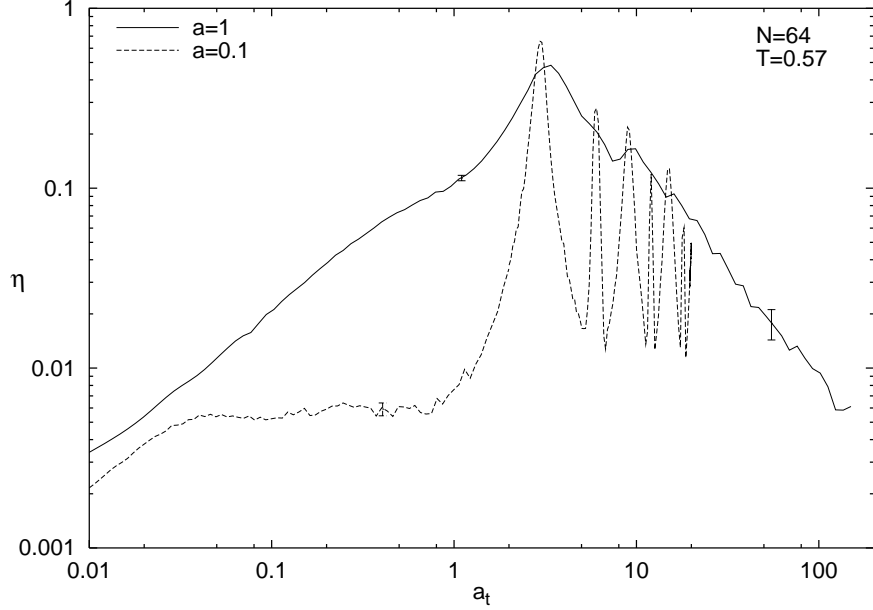


FIG. 4. The friction  $\eta(\langle \Phi \rangle_{h=0})$  as the function of the timelike lattice spacing  $a_t$ . The time scale of the fastest mode is  $\tau \approx 2$  and 0.22 for  $a = 1$  and 0.1, respectively, according to the perturbation expansion. Typical error bars appear on the curves both for the IR and UV regimes.

The non-trivial dependence of  $\eta$  on the temporal cutoff  $a_t$  is shown in Fig. 4. The curves were obtained by using the time evolutions corresponding to different values of  $a_t$  between 0.002 and 0.25. A blocking

$$\Phi(t) \rightarrow \Phi_{bl}(t) = \frac{1}{n} \sum_{k=-n/2}^{n/2-1} \Phi(t + ka_t) \quad (4.8)$$

was performed in time up to  $n = 2000$  and a discrete time equation of motion of the form Eq.(4.1) was reconstructed for the blocked trajectory. The "renormalized" real time trajectories generated by such a blocking procedure but starting with different initial values of the temporal cutoff  $a_t$  nicely agree.

One can distinguish two regimes separated by a crossover apparently independent of the lattice size, located at  $a_t \approx 0.2\tau$ . A scaling behavior is observed on the UV side, where  $\eta(a_t)$  tends to zero with a critical exponent close to 1 and the force being constant. This result should be independent of the actual blocking details. In the other regime, on the IR side  $\eta$  goes over first into an  $a_t$ -independent regime, corresponding to the saturation of the energy transfer from the OP and giving a stable, microscopic definition of the friction coefficient. Finally, in the far IR part a qualitatively different oscillatory behaviour sets in.

The location of the crossover from the UV scaling regime to the plateau can be understood by writing the fluctuation dissipation theorem in the corresponding discretised form:  $\langle \zeta^2 \rangle = 2\eta T/n a_t$ . The linearly increasing regime of  $\eta(n a_t)$  implies constant second moment for the noise. When  $\eta(n a_t)$  reaches the plateau the second moment of the noise decreases like  $1/n$ . The crossover therefore is located at the autocorrelation time scale of the noise.

A qualitative interpretation of the oscillatory IR regime can be based on the observed small amplitude beating phenomenon in the OP trajectory. This can be recognized by closer naked eye inspection of the left side of Fig.1, which persists further also on the right side. It is reflected in the OP autocorrelation function, too, since in the course of the blocking an interference effect occurs on the right hand side of Eq.(4.8) due to this regularity. This feature is relevant to the value of  $\eta(n a_t)$ , responsible for the decay of all kinds of fluctuations.

The appearance of peaks in  $\eta(n a_t)$  at both the maximal destructive and constructive interferences can be modeled semi-quantitatively by identifying the beating part of the OP-motion  $\text{Re}\delta\Phi = \text{Re}\delta\Phi_0 \exp(i\omega t)$  with the stationary solution of a single weakly damped driven harmonic oscillator,  $\delta\ddot{\Phi} + \eta\delta\dot{\Phi} + \omega_0^2\delta\Phi = f_0 \exp(i\omega t)$ . The blocking acts on the trajectory  $\delta\Phi(t)$  as  $\delta\Phi(t) \rightarrow u\delta\Phi(t)$ , where  $u = (\exp(i\omega n a_t) - 1)/i\omega n a_t$ . It does not change the relative phase of the driving force and of the blocked oscillation amplitude, leading to a relation between the parameters of the original and the blocked equation of motion:

$$-\omega^2 + i\eta\omega + \omega_0^2 = -\omega^2 u^2 + i\bar{\eta}\omega u + \bar{\omega}_0^2. \quad (4.9)$$

The friction coefficient for the blocked trajectory turns out to be  $\bar{\eta} = (\eta + \omega \text{Im}(u^2))/\text{Re}(u)$ . It is easy to see that  $\text{Re}(u)$  is vanishing at maximal constructive and destructive interferences. This provides singularities in  $\bar{\eta}$ . Whenever  $\text{Re}(u) = 0$  we have  $\text{Im}(u^2) = 0$  and numerator changes sign in the vicinity of the singularity. Thus  $\bar{\eta} > 0$  apart for a short time interval around the singularities where the non-harmonic features should stabilise the fluctuations and keep  $\bar{\eta} > 0$ , as observed in our simulation.

The  $a$  dependence appearing in Fig.4 arises from the following two effects. One is that for larger  $a$  the maximal oscillation frequency is smaller and the time resolution of the system becomes cruder. Another is that larger  $a$  represent bigger physical volume, many more soft modes and less harmonic system, which tends to invalidate the simple picture based on a single harmonic mode. As a result the effects of oscillatory nature will be smeared, as one clearly recognizes in the figure.

The quality of any proposed deterministic equation of motion (e.g. equations similar to Eq.(4.1) with zero on the right hand side), can be judged by the amplitude and the autocorrelation of its error term, *the noise term*  $\zeta$ . The amplitude of the noise was found at least two-three order of magnitude below the average level of the force as fitted to Eq. (4.1). The autocorrelation function of the noise of Eq. (4.1) appeared to be local, approximately of the form  $\langle \zeta_d(t)\zeta_d(t') \rangle \approx \delta''(t - t')$ . The status of the fluctuation-dissipation theorem will be investigated for more complex field theoretical systems in future investigations.

The selfconsistency of the definition of the temperature in Eq.(4.5) and also the establishment of the thermal equilibrium can be tested further by plotting histograms for the following quantities:

$$\begin{aligned} E_k &= \frac{1}{2} \left( \frac{d\Phi}{dt} \right)^2, \\ E_p &= \frac{\mu^2}{2} (\Phi - \langle \Phi \rangle_h)^2, \\ E_t &= E_k + E_p, \end{aligned} \quad (4.10)$$

where  $\mu^2$  is the slope of the force as the function of the order parameter, determined numerically. Typical results for the energy-histograms are shown in Fig.5. It shows perfect agreement of all slopes and good agreement with the expectations based on equipartition of the energy between the kinetic and the potential parts. We have checked for several temperatures, that the temperature determined by these histograms and from the  $|\mathbf{k}|$ -spectra of the kinetic energy agree. This piece of information is parallel to the recent detailed investigations of the thermalisation in  $(1+1)$ -dimensional  $\Phi^4$ -theories [18,19].

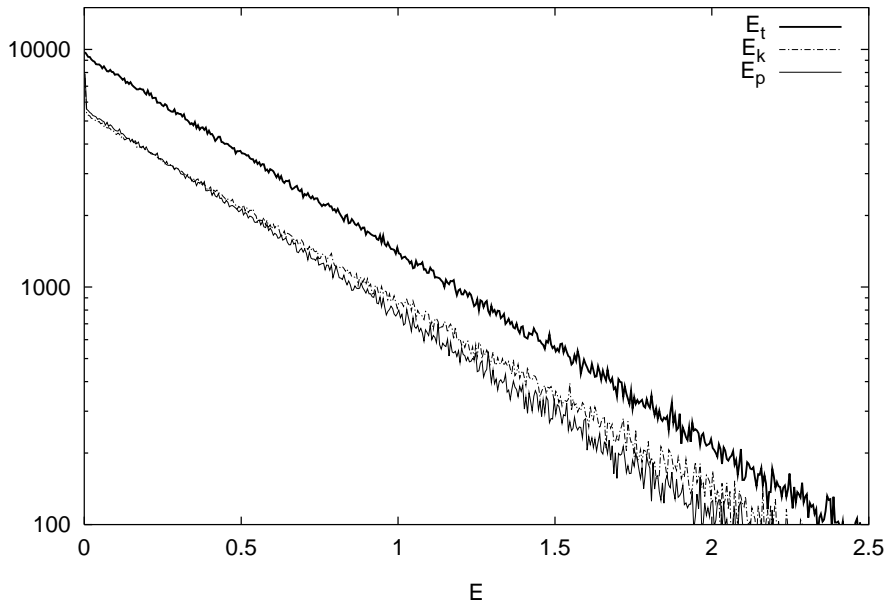


FIG. 5. The histogram of the energies  $E_t$ ,  $E_k$  and  $E_p$  of Eq.((4.10)) on a  $256 \times 256$  lattice with  $h = 2/\sqrt{6}$ .

It is worthwhile noting that the relaxation time from a given initial condition to the thermally distributed state like in this figure takes at least one order of magnitude longer time for systems in the symmetric phase compared to the spontaneously broken case. At higher energy density (temperature) one would expect larger collision frequency, therefore shorter thermalisation time. The opposite result hints to the importance of slow, soft modes, whose presence

is due to the symmetry breaking mechanism. We shall argue in the next Section that these modes are responsible for the realization of the Maxwell-cut in the potential term of the effective equation of motion for the OP. What we find remarkable is that these modes are present not only in the mixed phase but also near (meta)stable equilibria, among the dynamical fluctuations around the ordered vacuum in contrast to the massive perturbative excitation spectrum in the equilibrium.

We complete the analysis of this section with the remark, that after the transition to the stable vacuum shortly a thermalised distribution is recovered for the OP at somewhat increased temperature which agrees with the value given by the equipartition.

## V. JUMP FROM THE METASTABLE TO THE STABLE VACUUM

As it has been emphasized in the Introduction, there are (at least) two different descriptions of the transition from the metastable state to the stable one. The expansion around the lower pass, the “sphaleron” configuration yields a detailed space-time picture and the transition rate by means of the analytic continuation of the potential experienced by the OP near the (meta)stable position [4], [5].

Another possibility is to provide for the OP a probabilistic description, obtained by the elimination of all other degrees of freedom in some kind of blocking procedure. This description is based usually on some underlying Master equation for the probability distribution of the OP and the resulting Fokker-Planck equation [17]. The transition to the stable state appears in this approach formally as a tunneling solution of the Fokker-Planck equation. The probabilistic feature of the dynamics of the OP is supposed to arise from an averaging over the initial conditions.

In our simulation we find results analogous with the predictions of the probabilistic description by analysing the OP-motion starting from a single, well defined initial condition. One might wonder at this point if it is possible to understand the probabilistic tunneling of the OP by following the system from a unique initial condition. The self averaging in time can not be used for this argument since such a transition occurs only once during the evolution in a (quasi)irreversible manner.

In general, the effective equation of motion for  $\Phi(t)$  reflects the typical landscape of the microscopic potential energy functional around the actual point  $\Phi(\mathbf{x}, t)$  in the configuration space. The classical origin of what appears as a tunneling on the Fokker-Planck level must be the arrival of  $\Phi(\mathbf{x}, t)$  to the vicinity of some narrow valley opening up towards the stable vacuum. In traversing this valley the landscape changes and the typical fluctuations will be different from those felt in the metastable regime. The constants parametrising the effective equation of motion must reflect this change.

Our goal in this Section is to construct such a “classical tunneling” description of the transition to the stable state by carefully tracing the time evolution of the OP. This will be achieved by projecting the microscopic equation of motion onto the homogeneous mode and phenomenologically parametrising it similarly to Eq.(4.1).

As long as the system is far from the narrow valley of the instability the force is time independent and agrees with the force derived from the perturbative effective potential according to the part of Fig. 3 corresponding to  $\Phi > 0.9$ . When the external magnetic field brings the system closer to the entrance of the unstable valley, ( $\Phi \approx 0.8$ ), the soft modes start to be important. This is reflected in the slight glitch in the leftmost piece of the measured force law in Fig. 3. A sequence of glitches results in a situation depicted in Fig. 6. It shows the force acting on the OP in three successive time intervals preceding the event of tunneling for  $h = -0.04/\sqrt{6}$ . The  $f(\Phi)$  curves determined in the disjoint time subintervals coincide within error bars for all, but the last one. In this last interval preceding directly the transition to negative  $\Phi$  values, towards this direction the fitted force bends down and its average becomes (a small positive) constant. This is characteristic feature of the instant when the system finds the entrance into the unstable potential valley. The flattening of the potential, the vanishing of the force is an indication of the dynamical realization of the Maxwell-cut. The OP moves fast through the valley and the method of fitting the trajectory to Eq.(4.1) for finding the force fails due to the insufficient statistics.

The fluctuation moments depicted in Fig. 1 tell a bit more about this region. The increased values of the moments, the renormalized coupling constants in Wilsonian sense at vanishing momentum, indicate the enhanced importance of the soft interactions as the OP tunnels through the mean field potential barrier. This softening makes the OP fluctuating with larger amplitude. The valley of instability is in a surprising manner flatter than the typical landscape around equilibrium. The flatness along the motion of the OP (the mode  $\mathbf{k} = 0$  in momentum space) comes from the Maxwell-cut. The average curvature of the potential in the transverse directions, i.e. for modes with  $|\mathbf{k}| \neq 0$ , can be estimated by the second functional derivative of the two dimensional effective action with cutoff  $|\mathbf{k}|$ , which can be taken as  $\mathbf{k}^2 + V''_{\mathbf{k}}(\Phi)$ . The increased MS fluctuation of the OP corresponds to a decrease in  $V''_{\mathbf{k}=0}(\Phi)$  in the valley. It pushes down  $V''_{\mathbf{k}}(\Phi)$  also for small non-vanishing  $|\mathbf{k}|$ , in the low momentum regime which is expected to be the most influenced by the changing landscape.

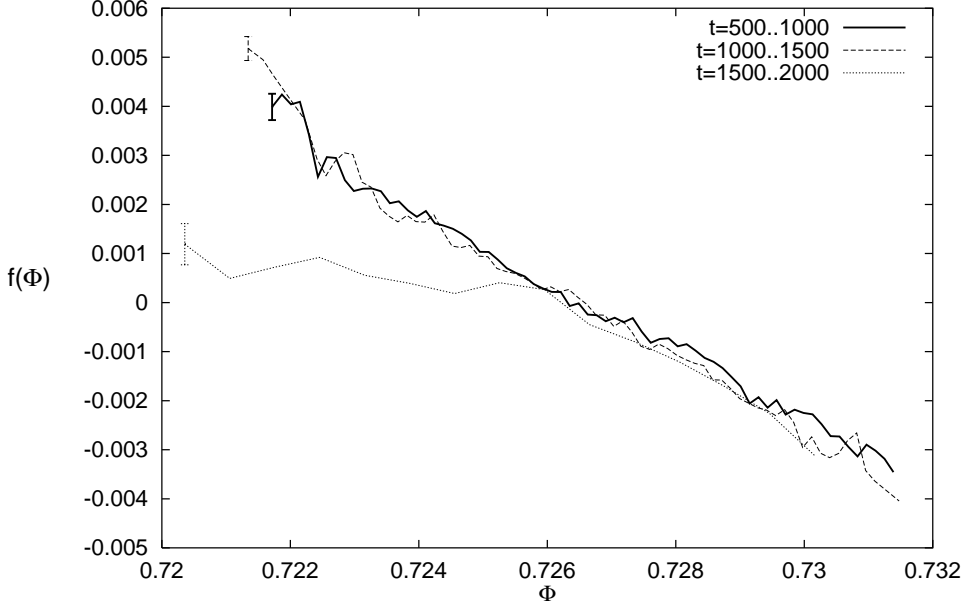


FIG. 6. The force  $f(\Phi)$  as the function of the order parameter on  $100 \times 100$  lattice with  $h = -0.04/\sqrt{6}$ . Each curve corresponds to time intervals of length  $500|m|^{-1}$ . The interval corresponding to the continuous curve ends  $1000|m|^{-1}$  before the transition, the long dashed curve refers to the next time interval and the short dashed curve is the force measured during the last time interval preceding the transition. One clearly observes the bending down left from the central OP-value in the metastable regime. Typical error bars are shown on the leftmost points of the three curves.

The lesson of Fig. 6 is that the potential itself should be considered as a fluctuating quantity. This helps to translate into more quantitative terms the above qualitative points. We discuss the projection of the microscopic equation of motion (2.5) onto the zero momentum sector,

$$0 = \ddot{\Phi} - \Phi + \Phi^3 + 3\overline{\varphi^2}^V \Phi + \overline{\varphi^3}^V - h \equiv \ddot{\Phi} + V'_{\text{inst}}(\Phi), \quad (5.1)$$

where the symbol  $\overline{\varphi^n}^V$  means the space average of  $\varphi^n$ , ( $\overline{\varphi}^V = 0, \Phi(t, \mathbf{x}) = \Phi(t) + \varphi(\mathbf{x}, t)$ ). The instant potential introduced in the second line contains a *deterministic* piece, which is the sum of the tree-level potential and of the slowly varying part the second and third moments (eg.  $(\overline{\varphi^n}^V)_{\text{det}}$ ). This last feature clearly appears graphically in Fig.1 and a simple model based on a two-phase model of the transition period will be constructed below to account for it. The remaining oscillating pieces of the moments provide the probabilistic fluctuating contribution to the instant potential:

$$V_{\text{inst}}(\Phi) = -h\Phi - \frac{1}{2}\Phi^2 + \frac{1}{4}\Phi^4 + (\overline{\varphi^3}^V)_{\text{det}}\Phi + \frac{3}{2}(\overline{\varphi^2}^V)_{\text{det}}\Phi^2 + \zeta_0\Phi + \frac{3}{2}\zeta_1\Phi^2. \quad (5.2)$$

The additive ( $\zeta_0$ ) and the multiplicative ( $\zeta_1$ ) noises are given by the differences

$$\begin{aligned} \zeta_0(t) &= \overline{\varphi^3}^V(t) - (\overline{\varphi^3}^V)_{\text{det}}, \\ \zeta_1(t) &= \overline{\varphi^2}^V(t) - (\overline{\varphi^2}^V)_{\text{det}}. \end{aligned} \quad (5.3)$$

Note that the breakdown of the time reversal invariance is expected to result from the cross-correlation between the two noises rather than the effective equation of motion (4.1) with a single noise and a friction term.

In order to gain more insight how this works we build into Eq.(5.1) the consequences of the mixed two-phase picture of the phase transformation. The microscopical basis for this picture is provided by the thermal nucleation whose quantitative discussion is given for completeness in the Appendix.

More specifically, we assume that the space can be splitted into sharp domains (neglecting the thickness of the walls in between), where the field is the sum of the constant background values  $\Phi_{0\pm}$  and the fluctuations  $\tilde{\varphi}_\pm$  around it,

$$\Phi_\pm(\mathbf{x}, t) = \Phi_{0\pm} + \tilde{\varphi}_\pm(\mathbf{x}, t). \quad (5.4)$$

We assume local equilibrium in both phases, based on the smooth evolution of the temperature as displayed in Fig.2.

The actual value of the order parameter is determined by the surface ratio  $p$  occupied by the stable phase:

$$\Phi = p\Phi_{0-} + (1-p)\Phi_{0+}. \quad (5.5)$$

Simple calculation then yields

$$\begin{aligned} (\overline{\varphi^2}^V)_{det} &= \frac{\Phi_{0+} - \Phi}{\Phi_{0+} - \Phi_{0-}} (\langle \Phi_-^2(\mathbf{x}, t) \rangle - \langle \Phi_+^2(\mathbf{x}, t) \rangle) + \Phi_{0+}^2 - \Phi^2 + \langle \tilde{\varphi}_+^2 \rangle, \\ (\overline{\varphi^3}^V)_{det} &= \frac{\Phi_{0+} - \Phi}{\Phi_{0+} - \Phi_{0-}} (\langle \Phi_-^3(\mathbf{x}, t) \rangle - \langle \Phi_+^3(\mathbf{x}, t) \rangle) + \langle \Phi_+^3(\mathbf{x}, t) \rangle - 3\Phi(\overline{\varphi^2}^V)_{det} - \Phi^3, \end{aligned} \quad (5.6)$$

where the expectation values should be read off the corresponding equilibria on the two sides of the transition. If one takes the values of  $\Phi_{0\pm}$ ,  $\langle \tilde{\varphi}_\pm^n \rangle$  from the respective equilibria determined in the same simulation, a quite accurate description of the shape of the two fluctuation moments arises in the whole transition region and its close neighbourhood. The RMS (root mean square) fluctuations found numerically on the transition part of the trajectory and its close neighbourhood are the following:

$$\sqrt{\overline{\zeta_0^2(t)}^t} = 0.0063(10), \quad \sqrt{\overline{\zeta_1^2(t)}^t} = 0.0054(10), \quad \text{for } N = 64 \quad (5.7)$$

(its magnitude increases with the size of the system). The magnitude of their equilibrium cross correlation was found  $\sim 10^{-5}$ . In this way, a simple explicit construction can be given for the effective noisy equation of the OP-motion, if the above pieces are supplemented by the correlation characteristics of the two kinds of noises.

As a corollary of this construction one can demonstrate the absence of the deterministic part of the acceleration of the order parameter in the transition period.

Substituting Eq.(5.6) into Eq.(5.1), one finds assuming vanishing noise terms,

$$\ddot{\Phi} + \left( -1 + \frac{\langle \Phi_+^3(\mathbf{x}, t) \rangle - \langle \Phi_-^3(\mathbf{x}, t) \rangle}{\Phi_{0+} - \Phi_{0-}} \right) \Phi + \frac{\Phi_{0+} \langle \Phi_-^3(\mathbf{x}, t) \rangle - \Phi_{0-} \langle \Phi_+^3(\mathbf{x}, t) \rangle}{\Phi_{0+} - \Phi_{0-}} - h = 0. \quad (5.8)$$

The average of the equations of motion in the respective equilibria,

$$\langle \Phi_\pm^3(\mathbf{x}, t) \rangle - \Phi_{0\pm} - h = 0 \quad (5.9)$$

implies the vanishing of the deterministic force in Eq. (5.8). This is the dynamical realization of the Maxwell-construction holding when the mixed phase model with local equilibrium is valid, and the fluctuating part of the force is negligible.

It is interesting to test the vanishing of the force also without neglecting the noisy part of the instant force. If the force is calculated from the full instant potential,  $V(\Phi)_{inst}$  in Eq. (5.2), it depends parametrically on the moments  $\overline{\varphi^2}^V(t)$  and  $\overline{\varphi^3}^V(t)$ . The approximate trajectory  $\Phi_{inst}(t)$ , obtained by minimising  $V(\Phi)_{inst}$  with respect to  $\Phi$ , where the moments are taken from the numerically determined time evolution, reproduced accurately the observed OP,  $\Phi(t)$  with the following RMS/unit time:

$$\sqrt{\overline{(\Phi(t) - \Phi_{inst}(t))^2}^t} = 0.0014(5), \quad \text{for } N = 64. \quad (5.10)$$

This construction interprets the OP-trajectory as a continuous deformation of the instant potential with the OP "sitting" permanently in the actual minimum. Notice that such motion is possible only if the OP continuously undergoes some sort of dissipation.

The vanishing of the acceleration was checked by comparing the computer generated OP trajectory in the transition region with a ballistic motion, in particular testing that the ratio  $h/\dot{\Phi}$  is nearly time and  $h$  independent for small enough  $h$ . The dynamical friction measured by the above ratio tends to a constant with decreasing  $h$  at fixed lattice size. Although the error for the  $\eta$ -value in each individual transition is rather small, the central values obtained in different runs fluctuate quite strongly, which leads eventually to a large error of the mean calculated as an average of runs with different initial configurations having the same energy density.

It is worth to note that the order of magnitude of these "renormalized", i.e. IR determined values of the friction coefficient agree with the peak value in Fig. 4 for  $N = 64$ . The "running" friction coefficient determined by the blocking in time, however, drops as  $nat$  is increased and takes extremely small values at  $nat \approx 20$ , the average time length of the ballistic fits for the transition. This serves an example for the dependence of the renormalization group flow on the details of the blocking. It remains to be understood whether the agreement between the peak value and the ballistic fit is an accident or follows from the internal dynamics.

## VI. CONCLUSIONS AND FUTURE DIRECTIONS

In this paper we have investigated in detail the decay of the false vacuum in a classical lattice field theory based exclusively on the effective theory of the order parameter. Two versions of the effective theory were reconstructed

from its trajectory derived from the microscopical equations of the theory. The first refers to the (meta)stable branch of the motion. The second one which takes into account the existence of a mixed phase during the transition period describes very well the transition together with its neighbourhood. The first equation has the form of conventional mechanical motion taking place in a dissipative noisy environment. The dissipation, the dynamical breakdown of the time inversion symmetry was found only for times longer then the minimal microscopic time scale of the system, the autocorrelation time of the noise. The dissipative nature of the second equation is realised, in the absence of any force term containing odd order time derivatives, by the presence of two cross-correlated noise terms.

As a corollary we find that the effective phenomenological OP-theory for the decay of the false vacuum through a narrow but flat valley demonstrates the presence of a dynamical Maxwell-construction.

The next possible directions of extending this work include the investigation of the effect of the quantum fluctuations on the large amplitude thermalisation of the one-component  $\Phi^4$  theory [20,21] and the extension of the results for models with continuous internal symmetry describing the dynamics of the inflaton field coupled to the Higgs+Gauge systems [22,23].

#### APPENDIX: THE NUCLEATION PICTURE

In this section we analyse the transition using the more conventional statistical approach of thermal nucleation theory.

From the study (on lattices up to  $N = 512$ ) of the detailed microscopical field configurations it turned out that the phase transformation starts by the nucleation of a single bubble of the stable ( $\Phi < 0$ ) phase. Late-coming further large bubbles are aggregated to it as well as the small size (consisting of  $n_{bubble} < 50 - 60$  joint sites) bubbles. Following the nucleation the expansion rate of the large bubble governs the rate of change of the order parameter. To a very good approximation each individual transition could have been characterised by a constant value of  $\dot{\Phi}$  in this interval. Two mechanisms are known to lead to this behavior. The first is scattering of hard waves (“particles”) off the bubble wall, while in the second the expansion velocity is limited by the diffusive aggregation of smaller bubbles [24]. The latter process seem to be the dominant in the kinetic Ising model [14].

The statistics of the “release” time of the supercritical bubble from the metastable state shows at first sight rather peculiar characteristics. The binned histogram for larger values of  $h$  shows an asymmetric peaked structure which apparently deviates from the exponential distribution characterising the thermal nucleation scenario (Fig.7). The very early transitions ( $t < t_{max}$ ) seem to be suppressed for small values of  $h$ . We expect they correspond to transitions, which happen before the system reaches the metastable state.

The fall-off for  $t > t_{max}$  starts nearly exponentially, but the histogram develops a very long tail when  $h \rightarrow 0$ . The bigger sample is used for estimating the probability distribution, the more suppressed is the weight of these events in the normalised distribution. In practice this means a longer time interval where a good linear fit can be obtained to the log-linear histogram. Eventually, the separation of a clean exponential signal is possible, and the slope can be compared with predictions of the nucleation theory.

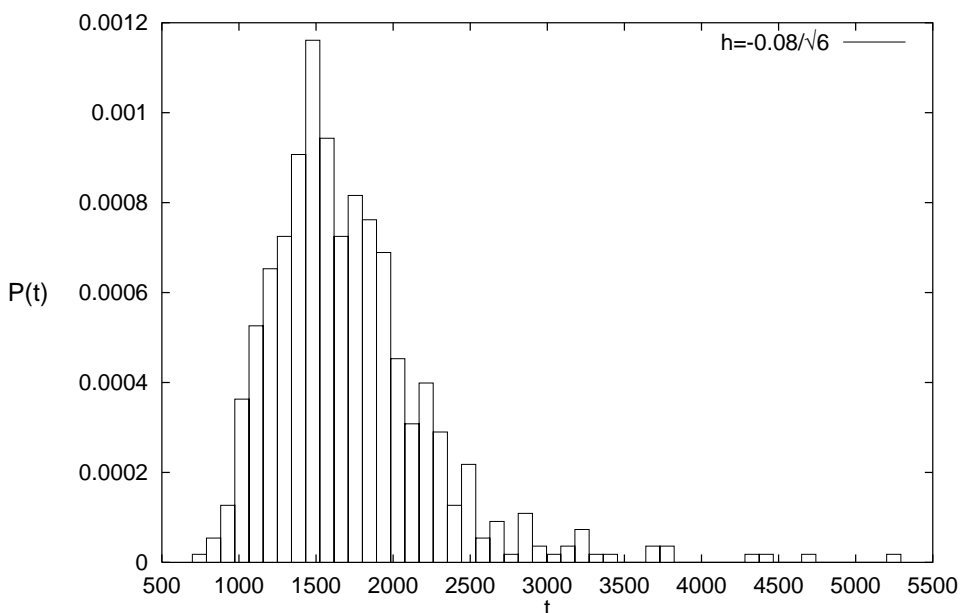


FIG. 7. The normalised "release" time histogram counting the frequency of a certain time moment-bin when the order parameter first takes a negative value. The figure represents the statistics based on 750 events at  $h = -0.08/\sqrt{6}$  on an  $N = 64$  lattice.

The nucleation rate is proportional to the volume of the system ( $N^2$ ). In Fig.8 we see evidence for the size independence of the transition rate per unit surface. The logarithm of this quantity can be estimated following the standard nucleation theory [4,5,25]:

$$\ln \Gamma = K - \frac{S_2}{T}. \quad (6.1)$$

$S_2$  is determined approximately by the action of the bounce solution, connecting the two vacua. In this investigation we have studied at fixed temperature the  $h$ -dependence of  $S_2/T$ , assuming the  $h$ -independence of  $K$ . In the thin wall approximation the following expression is used based on the tree level potential:

$$(S_2)_d = -2\pi\bar{r}^2 h \sqrt{\frac{6}{\lambda}} |m| + 8\sqrt{2}\pi\bar{r} \frac{|m|^3}{\lambda}, \quad (6.2)$$

(the first term on the right hand side corresponds to the volume energy of a bubble of radius  $\bar{r}$ , the second one to its surface energy). For the critical bubble size a very simple expression is obtained for the exponent of the rate in terms of dimensionless quantities:

$$\frac{S_2(\text{thin wall})}{T} = \frac{16\pi}{\sqrt{6}} \frac{|m|^5}{\lambda^{3/2}} \frac{1}{h_d T_d} = \frac{4\pi}{9} \frac{1}{hT}. \quad (6.3)$$

The linear dependence on  $1/h$  is fulfilled in our numerical calculations very well, but the predicted action is more than one order of magnitude larger than what can be derived from the slope of Fig.8:  $S_2/T(\text{measured}) \approx 0.1/(hT)$ . If one relaxes the thin wall approximation and solves numerically the two-dimensional bounce equation directly for several  $h$ , one finds  $S_2(\text{bounce})/T = 0.78/(hT)$ .

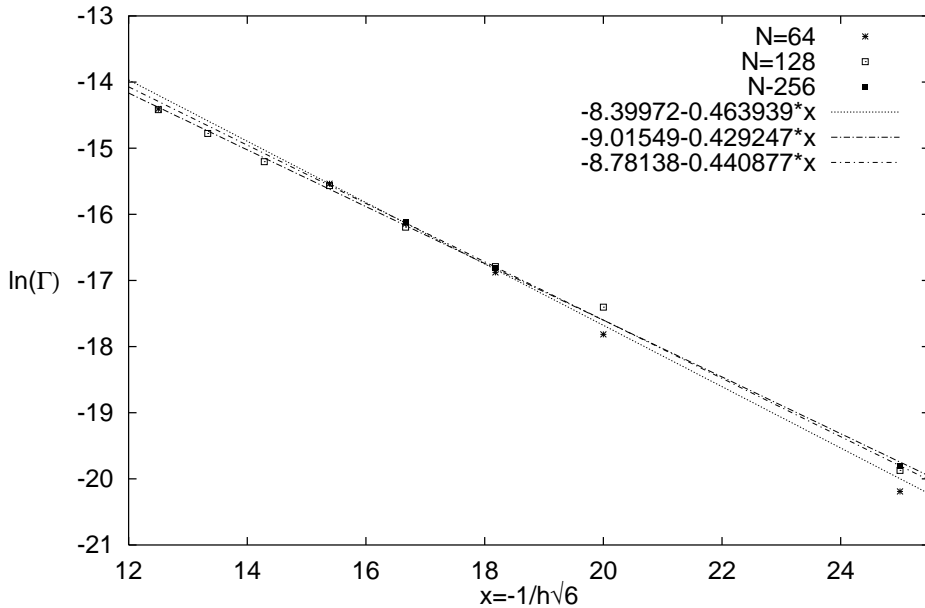


FIG. 8. Nucleation rate for unit lattice surface versus the reciprocal of the magnetic field for different lattice sizes. The error bars are smaller than the size of the symbols representing the data points.

Further improvement can be obtained by applying the temperature corrected effective potential in the bounce equation. We have determined the parameters of the  $T$ -dependent potential directly from our numerical calculation in the following way. The restoring force was measured for a certain  $h$  around both the stable and the metastable minima as described in section 4. Next an interpolating fit has been constructed of the form:  $h_{\text{eff}} + m_{\text{eff}}^2 \Phi + \lambda_3 \Phi^2 + \lambda_{\text{eff}}/6\Phi^3$ . It turned out that in the best fit  $\lambda_3 \approx 0$  is fulfilled always, while the values of the other coefficients are not too far from their tree level values. Then a bounce solution can be built on the corresponding (real!) potential which includes the temperature corrections. The final result is quite close to the measured value of the rate logarithm:  $S_2(T, \text{bounce})/T = 0.29/(hT)$ . The same real interpolation can be built on the neighbourhood of the minima of the

2-loop  $T$ -dependent effective potential, leading to  $S_2(T, \text{bounce})/T = 0.2/(hT)$ . By common experience in the surface tension simulations a factor of 2-3 difference in  $S_2$  is expected to arise relative to the mean field theory.

We conclude, that the finite temperature corrections are important for quantitative treatment of the nucleation rate within the thermal nucleation theory.

Next we turn to the discussion of the possible nucleation threshold at small  $h$ . The average “release time” increases for fixed lattice size with decreasing  $h$  (Fig.9). On a lattice of fixed size we found small  $h$  values for which we could not detect any transition, what makes very probable the existence of a threshold value of the external field  $h_{th}(N)$ . We did not attempt to locate this value beyond the simple hyperbolic fits to the few largest  $\langle t_{\text{release}} \rangle$  values. The value of  $h_{th}(N)$  remains stable when the smallest  $h$  is excluded from the fit, therefore we conclude that a threshold magnetic field exists similar to the case of the kinetic Ising model [14]. The value of  $h_{th}$  decreases when the lattice size is increased. Intuitively we expect  $h(\infty) = 0$ , but with the three lattices studied by us this conjecture cannot be demonstrated.

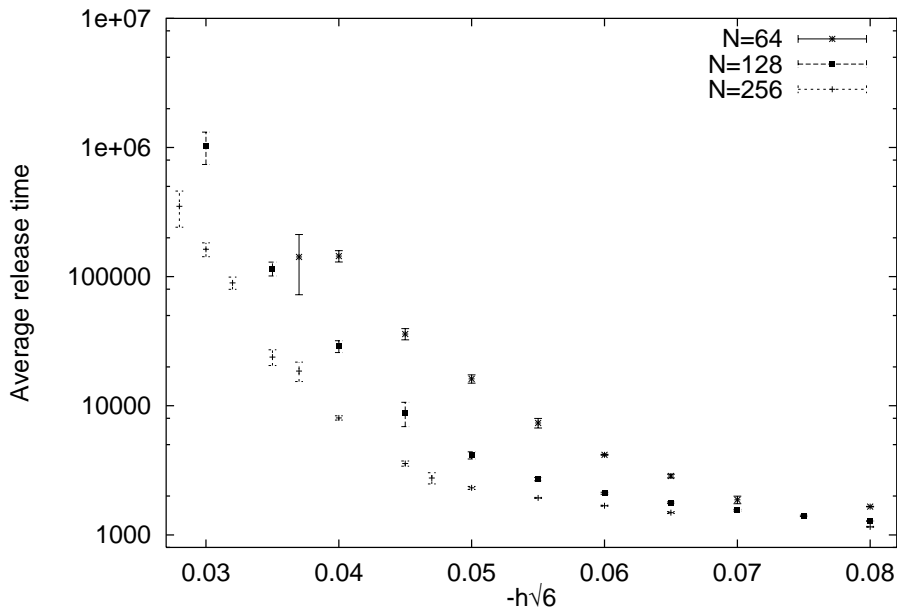


FIG. 9. The average “release” time as a function of  $h$  measured on  $N = 64, 128, 256$  lattices.

#### ACKNOWLEDGEMENTS

The authors are grateful for valuable discussions to C. Gagne, J. Hajdu, A. Jakovác, Z. Rácz and H.J. de Vega. They acknowledge the use of computing resources generously provided by the University of Bielefeld and the Dept. of Computer Science and the Inst. for Theoretical Physics of the Eötvös University. This research has been supported by CNRS and the Hungarian Science Fund (OTKA).

---

- [1] *Nucleation*, eds. A. Z. Zettlrmoyer, M. Dekker (Academic Press, N.Y. 1969); F. F. Abraham, *Homogeneous Nucleation Theory*, (Academic Press, N. Y. 1974); J. D. Gunton, M. San Miguel, Paramdeep Sahni, in *Phase Transitions and Critical Phenomena*, vol. 8, eds. C. Domb., J. L. Lebowitz (Academic Press, N. Y., 1983)
- [2] for a recent introduction, see D. Boyanovsky and H. de Vega, hep-ph/9909373, to appear in the Procs. of the IV Paris Colloquium on Cosmology
- [3] K. Binder, D. Stauffer, Adv. Phys. **25** (1976) 343
- [4] J. S. Langer, Ann. Phys. (NY) **41** (1967) 108
- [5] S. Coleman, Phys. Rev. **D15** (1977) 2929, S. Coleman and F. De Lucia, Phys. Rev. **D21** (1980) 3305
- [6] J. Alexandre, V. Branchina, J. Polonyi, Phys. Lett. **B445** (1999) 351
- [7] D. Boyanovsky, H.J. de Vega, R. Holman and J. Salgado, Phys. Rev. **D59** (1999) 125009
- [8] M. Alford and M. Gleiser, Phys. Rev. **D48** (1993) 2838
- [9] M. Gleiser and R.O. Ramos, Phys. Rev. **D50** (1994) 2441

- [10] M. Gleiser, Phys. Rev. Lett. **73** (1994) 3495
- [11] A. Berera, M. Gleiser and R.O. Ramos, Phys. Rev. **D58** (1998) 123508
- [12] E. Brézin and J. Zinn-Justin, Nucl. Phys. **B257** (1985) 867
- [13] K. Binder, Z. f. Physik **B43** (1981) 119
- [14] K. Binder and H. Müller-Krumbhaar, Phys. Rev. **B9** (1974) 2328
- [15] J.I. Kapusta, *Finite Temperature Field Theory*, (Cambridge University Press, Cambridge, 1989)
- [16] V. A. Miransky, Phys. Lett. **91B** (1980) 421, J. Polonyi, in the Proceedings of the *International School of Physics, Enrico Fermi*, Course CXXX, on Selected Topics in Nonperturbative QCD, Soc. It. di Fisica
- [17] N. G. van Kampen, *Stochastic Processes in Physics and Chemistry*, North Holland, 1981, see also A. Linde, Nucl Phys. **B372** (1991) 421
- [18] G. Parisi, Europhys. Lett. **40** (1997) 357
- [19] G. Aarts, G.F. Bonini and C. Wetterich HD-THEP-00-20, hep-ph/0003262
- [20] D. Boyanovsky, H.J. de Vega, R. Holman, D.-S. Lee and A. Singh, Phys. Rev. **D51** (1995) 4419
- [21] S. Khlebnikov and I.I. Tkachev, Phys. Rev. Lett. **77** (1996) 219, S. Khlebnikov, in Procs. of the Int. Conf. "Strong and Electroweak Matter '97", eds. F. Csikor and Z. Fodor, World Scientific, Singapore, 1998, pp. 69-88
- [22] J. Garcia-Bellido, D. Grigoriev, M. Kusenko and M. Shaposhnikov, Phys. Rev. **D60** (1999) 123504
- [23] D. Boyanovsky, D. Cormier, H.J. de Vega, R. Holman and S.P. Kumar, hep-ph/9801453
- [24] T.A. Witten and L.M. Sander, Phys. Rev. Lett. **47** (1981) 1400
- [25] M. Gleiser, G. C. Marques and R. O. Ramos, Phys. Rev. **D48** (1993) 1571